RESEARCH ARTICLE | FEBRUARY 18 2011

Molecular dynamics study of the melting curve of NiTi alloy under pressure

Zhao-Yi Zeng; Cui-E Hu; Ling-Cang Cai; Xiang-Rong Chen; Fu-Qian Jing

J. Appl. Phys. 109, 043503–043503-6 (2011)
https://doi.org/10.1063/1.3548936

Molecular dynamics study of the melting curve of NiTi alloy under pressure

Zhao-Yi Zeng,[1,2,a)] Cui-E Hu,[1,2] Ling-Cang Cai,[1] Xiang-Rong Chen,[2,3,b)] and Fu-Qian Jing[1,2]

[1]*National Key Laboratory for Shock Wave and Detonation Physics Research, Institute of Fluid Physics, Chinese Academy of Engineering Physics, Mianyang 621900, China*
[2]*College of Physical Science and Technology, Sichuan University, Chengdu 610064, China*
[3]*International Centre for Materials Physics, Chinese Academy of Sciences, Shenyang 110016, China*

(Received 18 October 2010; accepted 6 December 2010; published online 18 February 2011)

The melting curve of NiTi alloy was predicted by using molecular dynamics simulations combining with the embedded atom model potential. The calculated thermal equation of state consists well with our previous results obtained from quasiharmonic Debye approximation. Fitting the well-known Simon form to our T_m data yields the melting curves for NiTi: $1850(1+P/21.938)^{0.328}$ (for one-phase method) and $1575(1+P/7.476)^{0.305}$ (for two-phase method). The two-phase simulations can effectively eliminate the superheating in one-phase simulations. At 1 bar, the melting temperature of NiTi is 1575 ± 25 K and the corresponding melting slope is 64 K/GPa. © *2011 American Institute of Physics*. [doi:10.1063/1.3548936]

I. INTRODUCTION

It is a fundamental issue to investigate the behaviors of transition metals and their alloys under high pressure (P) and high temperature (T) in material physics and geophysics. The thermal properties, in particular their melting behaviors, have attracted much attention in the past decade.[1–12] The melting of Fe under extreme conditions can be used to determinate the temperature at the Earth's inner-outer core boundary,[8,9] which is crucial to constrain the geophysical and geochemical models for the Earth's core. However, obtaining the melting curves for the transition metal is a challenge to experimentalists and theorists. The melting curves are of significant difference among static compression measurements,[3,4,11,13–16] shock data[17–19] and molecular dynamics (MD) simulations.[8,20–22] In the latest report, Dewaele *et al*. considered that under high pressures the melting temperature (T_m) of Ta was underestimated in diamond anvil cell (DAC) experiments.[23] But the T_m data in their experiments were not measured but calculated. Ruiz-Fuertes *et al*. also obtained the new T_m data of Ta by using scanning electron microscopy.[11] Their DAC melting data were in excellent agreement with earlier measurements (low melting slopes of the transition metal) and confirmed the validity of earlier experimental techniques. But the strong divergence between DAC and Sock-Wave measurements in transition metals still remains inconclusive.

The transition metal alloys are promising functional materials which are well used for engineering purpose. For nitinol (NiTi), a well known shape memory alloy, is widely used in the aeronautical, medical, and seismological areas. In the last few years, the scientific investigations for NiTi have been made extensively, including the structural properties,[24–26] phase stabilities,[24,27–31] elastic properties,[28,31–34] thermodynamics,[31,35–37] and martensitic transformation path.[27,28,30] In our previous work, we investigated the solid-solid phase transitions of NiTi by first-principle calculations.[31] To construct the complete phase diagram, the research of the solid-liquid boundary (melting curve) becomes very important. As far as we know, the melting curve of NiTi under high pressure is not known.

There are four different phases that have been observed throughout the martensitic transformation of NiTi: B2, R, B19, and B19′. Above room temperature, NiTi is stable in austenitic B2 phase (CsCl-type, *Pm-3m*). As the temperature decreases, the high temperature austenitic B2 phase undergoes a displacive structure transformation to intermediate B19 (*Pcmm*) or R (*P*-3) phase at about 293 K, and then transforms to the low-temperature martensite B19′ phase (monoclinic, $P2_1/m$) near 273 K.[38] In present work, we investigated the melting curve of NiTi, so the MD simulations were performed on B2 structure. We hope the study can contribute to understand the high pressure behavior of NiTi alloy. In Sec. II, we give a description of the computational methods. The results and detailed discussions are presented in Sec. III. The short conclusions are summarized in the last section.

II. DETAILS OF CALCULATIONS AND MODELS

MD simulation is a direct simulation technique at the atomic level. It consists of solving a set of differential equations obtained by applying the Newton laws overall particles of the system. In present MD simulations, three-dimensional periodic boundary conditions were applied. And we applied two methods to simulate the melting behavior of NiTi, i.e., the one-phase method and the two-phase method which have been frequently used in studying other metals.[7,22,39,40] For the first method, we heated all of the atoms in the cell until melting. From our tests on size dependence of melting point, we found that the difference of melting point obtained from 1024 atoms and 2000 atoms are less than 100 K in the whole range of pressure. So we are sure that 2000 atoms are sufficient for simulating the melting curve of NiTi at all pressures of interest. For the latter method, to construct initial configuration of solid-liquid coexistence, we heated 2000 atoms up to 3000 K (far beyond the melting point) in *NVE* ensemble.

a)Electronic mail: zhaoyizeng@126.com.
b)Electronic mail: xrchen@126.com.

Then we merged the liquid and solid parts in the box along *z*-axis. As a result, the coexistence phase (including 4000 atoms) containing a solid-liquid interfaces was constructed. This box was used as the initial configuration for further simulations. In both methods, the isothermal-isobaric *NPT* ensemble was used to achieve constant temperature and pressure. The Verlet leapfrog integration algorithm is used with a time step of 0.5 fs. The total simulation time steps were 10 0000, which was tested to be sufficient for current coexistent simulations. The first 60 000 steps were used for equilibrium, and the last 40 000 steps for statistical average of properties.

The embedded atom model (EAM) potential assumes that the crystal energy is the sum of a pairwise potential and an energy required to embed an atom into a local medium with a given electron density. By normalizing the EAM potentials and introducing an EAM alloy model, Zhou and Wadley *et al*. developed a procedure to generalize the EAM potentials.[41,42] This generalized EAM potential has been extended to enable calculations of many alloys, including NiTi alloy. In EAM, the total energy E of the crystal can be expressed as

$$E = \frac{1}{2}\sum_{i,j,i\neq j}\Phi_{ij}(r_{ij}) + \sum_{i}F_i(\rho_i)\,, \tag{1}$$

where Φ_{ij} represents the pair energy between atoms i and j separated by r_{ij}, and F_i stands for the embedding energy to embed an atom i into a local site with electron density ρ_i.

$$\rho_i = \sum_{i,j,i\neq j} f_j(r_{ij})\,, \tag{2}$$

where $f_j(r_{ij})$ is the electron density at the site of atom i arising from atom j at a distance r_{ij} away. To fit such an EAM potential set, the generalized pair potentials were chosen to have the form

$$\Phi(r) = \frac{A\exp[-\alpha(r/r_e-1)]}{1+(r/r_e-\kappa)^{20}} - \frac{B\exp[-\beta(r/r_e-1)]}{1+(r/r_e-\lambda)^{20}}\,, \tag{3}$$

where r_e is the equilibrium spacing between nearest neighbors, A, B, α and β are four adjustable parameters, κ and λ, are two additional parameters for the cutoff. The electron density function is taken with the same form as the attractive term in the pair potential

$$f(r) = \frac{f_e\exp[-\beta(r/r_e-1)]}{1+(r/r_e-\lambda)^{20}}\,. \tag{4}$$

Using the alloy model,[43] the pair potential between different species a and b is constructed as

$$\Phi^{ab}(r) = \frac{1}{2}\left[\frac{f^b(r)}{f^a(r)}\Phi^{aa}(r) + \frac{f^a(r)}{f^b(r)}\Phi^{bb}(r)\right]. \tag{5}$$

To have embedding energy functions that can work well over a wide range of electron density, three equations are separately fitted to different electron density ranges. These equations are

$$F(\rho) = \sum_{i=0}^{3}F_{ni}\left(\frac{\rho}{\rho_n}-1\right)^i, \rho<\rho_n, \rho_n = 0.85\rho_e, \tag{6}$$

$$F(\rho) = \sum_{i=0}^{3}F_{i}\left(\frac{\rho}{\rho_e}-1\right)^i, \rho_n\le\rho<\rho_0, \rho_0 = 1.15\rho_e, \tag{7}$$

$$F(\rho) = \sum_{i=0}^{3}F_{e}\left[1-\ln\left(\frac{\rho}{\rho_s}\right)^{\eta}\right]\left(\frac{\rho}{\rho_s}\right)^{\eta}, \rho_0\le\rho. \tag{8}$$

The parameters for NiTi alloy are shown in previous work by Zhou and Wadley *et al*.[41,42]

III. RESULTS AND DISCUSSION

Firstly, we have performed MD simulations for the thermal equation of state (EOS) of B2-NiTi under pressure. This way is a direct test of the accuracy of present MD simulations. At ambient conditions, though the obtained equilibrium volume 28.02 Å^3 is 2.44% larger than the experimental datum 27.35 Å^3,[44] the result is reasonable and acceptable. The calculated isotherms at different temperatures are plotted in Fig. 1. There are no experimental values under high pressure and high temperature for comparison. So we compare with our previous results calculated from quasiharmonic Debye approximation.[31] Generally, the present MD results are in agreement with our previous work. The bulk modulus B and its pressure derivative B' can be obtained directly from the P-V relations:

$$B = -V\partial P/\partial V,\ B' = \partial B/\partial P. \tag{9}$$

The parameters from present MD simulations are shown in Fig. 2, compared with our previous calculations.[31] At 298 K and 1 bar, the bulk modulus B from MD is 135 GPa, which is smaller than our previous result 151 GPa at 300 K and zero pressure,[31] but agree with the experimental data 140.3 GPa.[45] It can be seen that the bulk modulus B decreases dramatically with the increasing temperature.

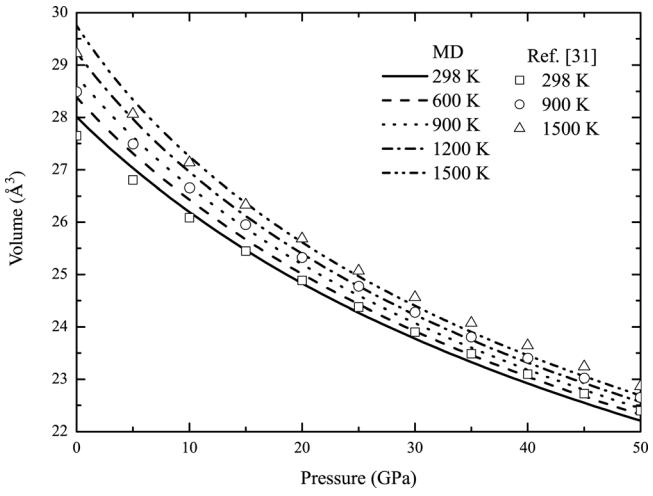

FIG. 1. The isotherms at different temperatures. The open symbols are the previous theoretical data from quasiharmonic Debye approximation (see Ref. 31).

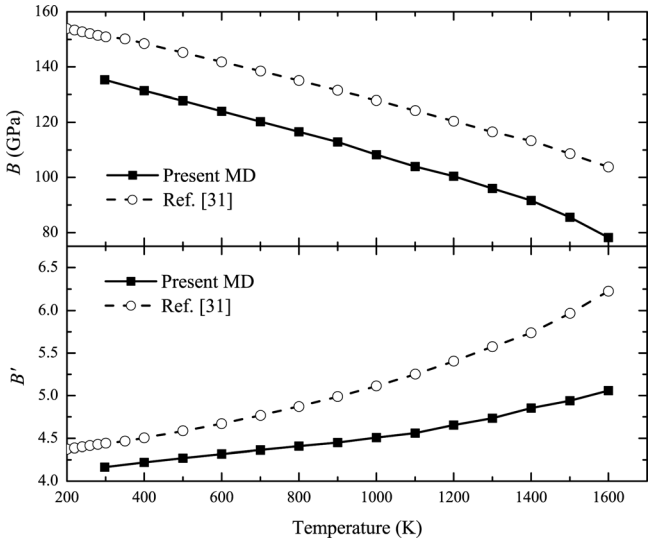

FIG. 2. The bulk modulus B and its pressure derivative B' of NiTi versus temperature at zero pressure.

For the pressure derivative B', the present result at 298 K and 1 bar is 4.16, which is also smaller than the previous result 4.44.[31] As temperature increases, the B' in present work increases slightly.

Thermal expansion of a solid is a direct consequence of the anharmonicity of lattice vibrations. It can manifest the anharmonic nature of interatomic forces. For the calculations of melting properties, the response of a potential to temperature is crucial in simulating the anharmonic nature of the interatomic forces in a solid. We have calculated the volumes of NiTi in a wide range of pressure and temperature. The lattice volumes as functions of temperature at different pressures are shown in Fig. 3, together with the data at 0 GPa from quasiharmonic Debye approximation.[31] It can be seen that though the present results at 1 bar are a little larger than that from quasiharmonic Debye approximation, the normalized volume expansion V/V_0 (the insert of Fig. 3) agree well with the previous results.

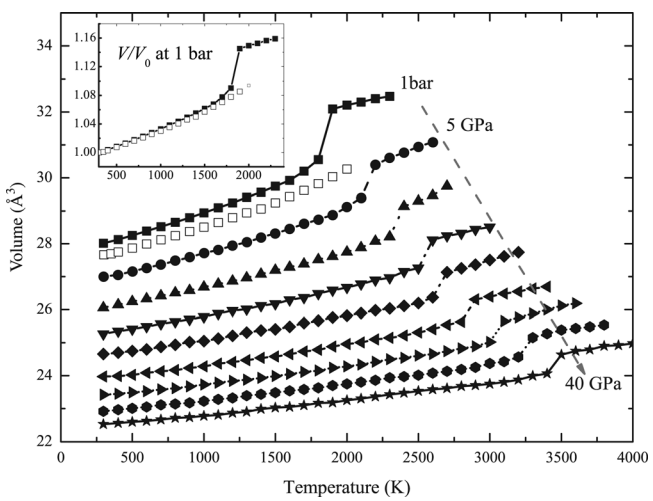

FIG. 3. The volume at different pressures (1 bar and from 5 GPa to 40 GPa with 5 GPa interval) versus temperature, The insert of the figure is the normalized volume ratio as a function of temperature at 1 bar. The open squares are previous theoretic data (see Ref. 31).

The volume thermal expansivity

$$\alpha_V = \frac{1}{V}\left(\frac{\partial V}{\partial T}\right)_P \tag{10}$$

can be determined from the equilibrium volume variation with respect to temperature at each pressure. The thermal expansivity of NiTi as functions of temperature at different pressures is shown in Fig. 4. At ambient condition, the volume thermal expansion is 3.08×10^{-5} K^{-1}, corresponding to the linear thermal expansion 1.03×10^{-5} K^{-1}, which is consistent with the earlier experimental datum 1.1×10^{-5} K^{-1}.[46] The thermal expansivity increases with the increasing temperature. When the temperature is close to the T_m, the thermal expansivity increases significantly, indicating the melting. As pressure rises, the anharmonicity from temperature are suppressed quickly.

When studying the melting of alloy, it is important to know whether the system is a eutectic alloy. The eutectic temperature of the system is always smaller than the melting temperature, e.g., Fe-S systems.[47,48] The composition Ti/(Ni + Ti) = 0.5 in Ni-Ti system is far away from the eutectic composition.[49] In present simulations, the NiTi alloy is an intermetallic compound not a mixture. The atoms Ni and Ti construct a periodic crystal. So the NiTi in this work is a noneutectic alloy. The T_m datum is usually identified by studying the variation in either the thermodynamic properties or structural properties. The first-order melting transition of NiTi can be identified at certain temperature where the mean volume undergoes a sudden upward jump, as marked in Fig. 3. From Fig. 3, one can see that the volume jumps between 1800 and 1900 K at ambient pressure, indicating the melting. As the pressure increases, it is worth noting that the melting point increases.

The atomic pair-correlation functions $g(r)$ is computed to examine the structural properties of the simulated system. The $g(r)$ is the probability of finding another atom at a distance between r and $r + dr$ from a specified atom. The solid phase is characterized by periodic oscillations of the average number density and shows several well-defined peaks after

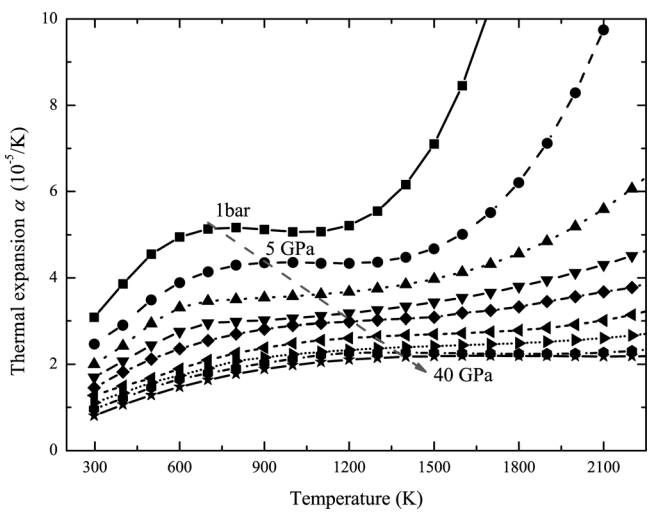

FIG. 4. Thermal expansivity of NiTi as a function of temperature from 1 bar up to 40 GPa.

the first peak. For liquid phase, the $g(r)$ shows large fluctuations at small distances and approaches unity at larger distances indicating the short-range order and long-range disorder. We have calculated the $g(r)$ for Ni-Ti, Ti-Ti, and Ni-Ni. The results around melting point at ambient pressure and $T = 298$, 1800, 1900, and 2000 K are shown in Fig. 5. The $g(r)$ shows distinct peaks at 300 K, indicating the solid structure. With temperature increasing up to 1800 K, the distinct peaks start to vanish and the system tends to liquefy. At 1900 K, the $g(r)$ shows a lower first peak and a smoother curve, indicating a liquid structure. The $g(r)$ at 2000 K is similar to that at 1900 K, which confirms that the system has melted completely at 1900 K. So we can estimate that the T_m is 1850 ± 50 K. We also calculated the pair-correlation functions at different pressures, and obtained the T_m data under high pressure. Fitting the well-known Simon functional form to present T_m values yields our melting curves for NiTi:

$$T_{m1-phase}(P) = 1850\left(1 + \frac{P}{21.938}\right)^{0.328}. \quad (11)$$

According to the melting curve, we can obtain the melting slope dT_m/dP under pressure. At ambient pressure, the dT_m/dP is about 50 K/GPa.

In the two-phase method, at a fixed pressure, when system temperature is below the melting point, the interfaces will move toward the liquid part, i.e., the liquid layer adjacent to solid will be continuously crystallized to be solid. Whereas, when system temperature is above melting point, the interfaces will move toward the solid parts, i.e., the solid parts will melt to be liquid. The configurations at 1 bar are shown in Fig. 6(a), (b), and 6(c). For the liquid part in Fig. 6, the atoms Ni and Ti are disordered, which indicates that the NiTi melted completely. In the solid part, the Ni and Ti remains alloyed. For the interface, there is a mixture of solid and liquid.

To monitor the simulations there are a number of tools, including the mean square displacement and the planar density. The planar density is defined as the number of atoms

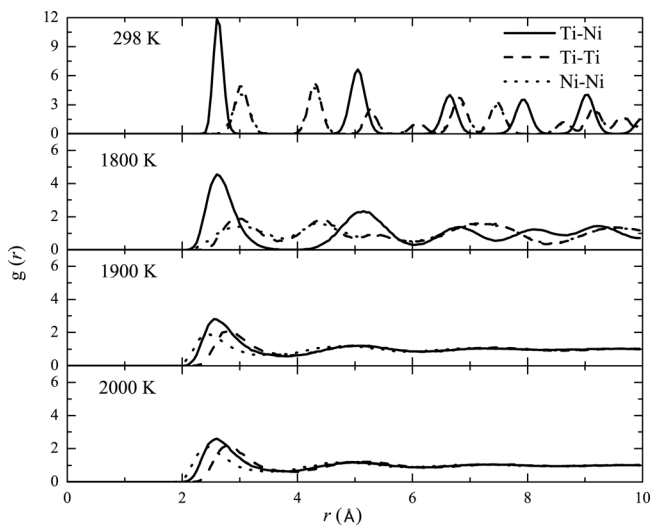

FIG. 5. The pair-correlation functions $g(r)$ at $P = 1$ bar and $T = 298$, 1800, 1900, and 2000 K. At $T = 298$ K, the $g(r)$ shows distinct peaks, indicating a solid structure. At $T = 1800$ K the configuration tends to liquefy. At $T = 1900$ and 2000 K, the smooth curve of the $g(r)$ emphasizes a liquid structure.

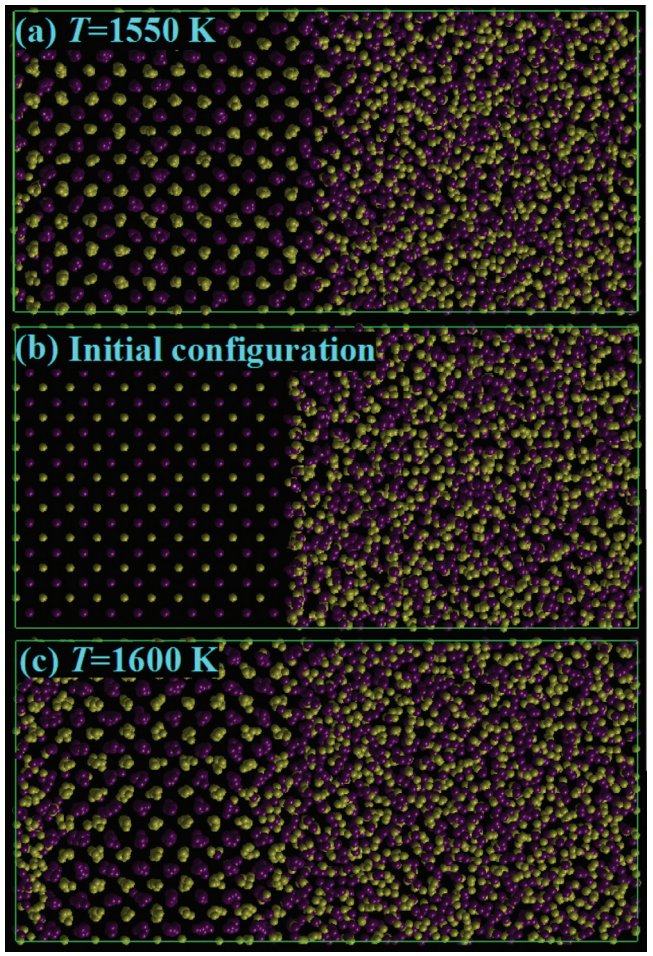

FIG. 6. (Color online) The configuration of solid-liquid coexistence phase at 1 bar; the purple and yellow spheres represent Ni and Ti atoms, respectively.

presented in a slice of the simulation box cutting parallel to the solid-liquid interface. As is shown in Fig. 7, in the solid region this planar density is a periodic function, while in the liquid region it is simply a random number fluctuating around an average value. By narrowing the interval of the temperature, the T_m datum can be estimated at the fixed pressure in the simulation. From Fig. 7, it can be seen that at 1 bar, the T_m is 1575 ± 25 K, which agrees well with the experimental datum 1583 K.[50] We repeated the steps at different pressures, and then we can obtain the whole melting curve under high pressure. The Simon functional form to two-phase T_m data is as follows:

$$T_{m2-phase}(P) = 1575\left(1 + \frac{P}{7.476}\right)^{0.305}. \quad (12)$$

The dT_m/dP at 1 bar is about 64 K/GPa from two-phase simulations, which is larger than that from one-phase simulations.

We also obtained the melting curves of pure Ni and Ti, as they can verify the accuracy of the potential in simulations and confirm the validity of the melting curve of NiTi. The structure of the pure metal Ni in simulations were treated with fcc (face-centered cubic) structure, as it keeps fcc phase under high pressure. For the pure metal Ti, at ambient condition, it is in the hexagonal-close-packed (hcp) crystal structure, and then transforms to a body-centered-cubic (bcc) structure when

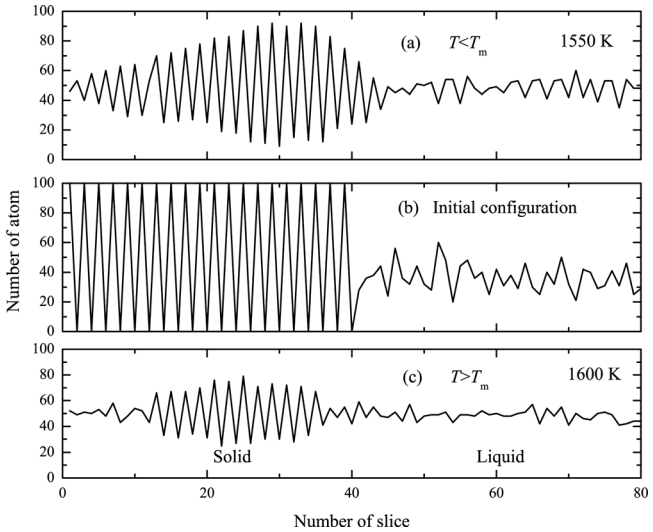

FIG. 7. Density profile for the coexistence configuration. The solid phase is identified by periodic oscillations of the density, while the density of the liquid phase fluctuates with much smaller amplitude. (a) The moving of interfaces toward liquid part when $T < T_m$; (b) the initial configuration; (c) the moving of interfaces toward solid parts when $T > T_m$.

the temperature is higher than 1155 K.[51] From the phase diagram of Ti, we can see that the stable phase under high pressure and high temperature is bcc-Ti.[52] So we simulated the melting of bcc-Ti. By using the two-phase simulation, the obtained melting curves of Ni and Ti are as follows:

$$T_{m-Ni}(P) = 1550\left(1 + \frac{P}{23.955}\right)^{0.620}, \quad (13)$$

$$T_{m-Ti}(P) = 1800\left(1 + \frac{P}{15.615}\right)^{0.447}. \quad (14)$$

At ambient pressure, the dT_m/dP for pure Ni and Ti are 40 and 51 K/GPa, respectively. The melting slope of Ni in present work agree with the value obtained according to the Lindemann law,[1] but larger than the DAC datum 25 K/GPa.[4]

The melting curves for NiTi, pure Ni and Ti are shown in Fig. 8, together with the DAC experimental data for pure Ni and Ti.[4] Unfortunately, there are no experimental or other theoretical results for NiTi. Therefore experiments are urgently needed to further determine the melting curve of NiTi. The present T_m data for Ni and Ti are larger than the DAC data under high pressure, but generally agree with the theoretical data for Ni by our group.[53] For the melting curves of NiTi, as pressure increases, the melting slop of two-phase method decreases much faster than that of one-phase method. All the T_m data from one-phase simulations are smaller than that from two-phase simulations, which indicating the superheating in one-phase simulations. In the one phase method the periodic boundary conditions were applied, the effect of free surfaces is removed and the long-range order of the crystalline structure is maintained up to certain temperature above the equilibrium melting temperature, so the superheating in one-phase simulations occurs. According to the modern theory of melting,[54,55] the superheated T_m of a crystal can be corrected by a certain melting mechanism. The corresponding superheating melting of

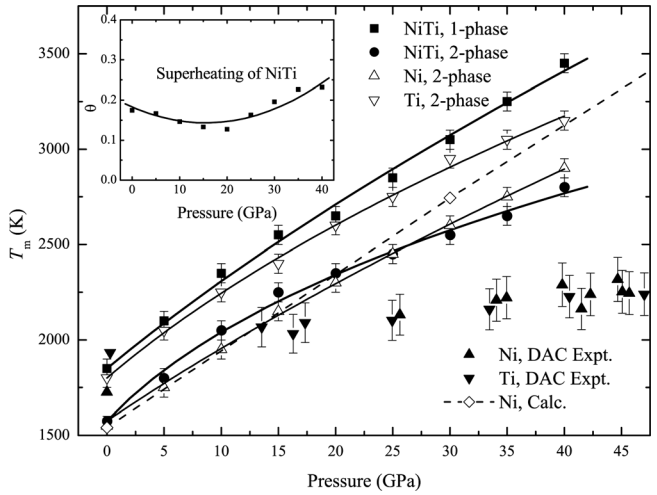

FIG. 8. Calculated melting curves from one-phase (solid squares) and two-phase (solid circles) simulations (the solid and dashed lines are the melting data fitted with Simon equation). The solid triangles with error bar represent the experimental data for pure Ni and Ti (see Ref. 4), and the theoretical data for Ni (see Ref. 53). The insert of the figure is the superheating as a function of pressure.

some crystalline solids at ambient pressure can be concluded as $\theta = T/T_{m0} - 1$, where T_{m0} is the conventional melting temperature for the bulk phase. The superheating for many metals in MD one-phase simulations is around 0.1–0.3.[54,55] By comparing the one-phase and two-phase results, one can observe that the superheating ($\theta = T_{m1-phase}/T_{m2-phase} - 1$) is obvious (shown in the insert of Fig. 8). With the pressure increasing, it decreases from 0.17 at 1 bar to 0.13 at 20 GPa, and then increase quickly to 0.23 at 40 GPa. The superheating effect can be eliminated by simulating a coexistent system with a solid-liquid interface.

IV. CONCLUSIONS

In summary, we have investigated the melting curve of NiTi under high pressure from classical MD simulations combining with the EAM potential. The thermal equation of state of NiTi is very successful in reproducing our previous data from quasiharmonic Debye approximation over a wide range of pressure and temperature. Fitting the well-known Simon form to our T_m values yields the melting curves for NiTi: $1850(1 + P/21.938)^{0.328}$ (for one-phase method) and $1575(1 + P/7.476)^{0.305}$ (for two-phase method). The two-phase simulations can eliminate the superheating in one-phase simulations effectively. The melting temperature of NiTi at 1 bar is 1575 ± 25 K and the corresponding melting slope is 64 K/GPa.

ACKNOWLEDGMENTS

The authors would like to thank Prof. Yan Bi for the helpful discussions. This research is supported by the National Natural Science Foundation of China under Grant Nos. 10776029 and 10776022, and the Specialized Research Fund for the Doctoral Program of Higher Education under Grant No. 20090181110080.

[1] D. Errandonea, J. Appl. Phys. **108**, 033517 (2010).
[2] S. Japel, B. Schwager, R. Boehler, and M. Ross, Phys. Rev. Lett. **95**, 167801 (2005).
[3] D. Errandonea, Physica B **357**, 356 (2005).

[4]D. Errandonea, B. Schwager, R. Ditz, C. Gessmann, R. Boehler, and M. Ross, Phys. Rev. B **63**, 132104 (2001).
[5]L. Vočadlo and D. Alfè, Phys. Rev. B **65**, 214105 (2002).
[6]Z.-Y. Zeng, X.-R. Chen, J. Zhu, and C.-E. Hu, Chin. Phys. Lett. **25**, 230 (2008).
[7]Z.-L. Liu, L.-C. Cai, X.-R. Chen, and F.-Q. Jing, Phys. Rev. B **77**, 024103 (2008).
[8]D. Alfè, M. J. Gillan, and G. D. Price, Nature **401**, 462 (1999).
[9]D. Alfè, M. J. Gillan, and G. D. Price, Contemp. Phys. **48**, 63 (2007).
[10]D. Errandonea, Nature Mater. **8**, 170 (2009).
[11]J. Ruiz-Fuertes, A. Karandikar, R. Boehler, and D. Errandonea, Physics of the Earth and Planetary Interiors **181**, 69 (2010).
[12]C. J. Wu, P. Söderlind, J. N. Glosli, and J. E. Klepeis, Nature Mater. **8**, 223 (2009).
[13]D. Errandonea, J. Phys.: Condens. Matter **16**, 8801 (2004).
[14]D. Errandonea, J. Phys. Chem. Solids **67**, 2017 (2006).
[15]D. Errandonea, M. Somayazulu, D. Hausermann, and H. K. Mao, J. Phys.: Condens. Matter **15**, 7635 (2003).
[16]D. Santamaría-Pérez, M. Ross, D. Errandonea, G. D. Mukherjee, M. Mezouar, and R. Boehler, J. Chem. Phys. **130**, 124509 (2009).
[17]J. M. Brown and J. W. Shaner, *Shock Waves in Condensed Matter* (Elsevier, New York, 1984).
[18]R. S. Hixson, D. A. Boness, J. W. Shaner, and J. A. Moriarty, Phys. Rev. Lett. **62**, 637 (1989).
[19]X.-L. Zhang, L.-C. Cai, J. Chen, J.-A. Xu, and F.-Q. Jing, Chin. Phys. Lett. **25**, 2969 (2008).
[20]A. B. Belonoshko, L. Burakovsky, S. P. Chen, B. Johansson, A. S. Mikhaylushkin, D. L. Preston, S. I. Simak, and D. C. Swift, Phys. Rev. Lett. **100**, 135701 (2008).
[21]C. Cazorla, D. Alfè,and M. J. Gillan, Phys. Rev. Lett. **101**, 049601 (2008).
[22]A. B. Belonoshko, S. I. Simak, A. E. Kochetov, B. Johansson, L. Burakovsky, and D. L. Preston, Phys. Rev. Lett. **92**, 195701 (2004).
[23]A. Dewaele, M. Mezouar, N. Guignot, and P. Loubeyre, Phys. Rev. Lett. **104**, 255701 (2010).
[24]X. Huang, G. Ackland, and K. Rabe, Nature Mater. **2**, 307 (2003).
[25]J. M. Wills and B. R. Cooper, Phys. Rev. B **36**, 3809 (1987).
[26]S. Prokoshkin, A. Korotitskiy, V. Brailovski, S. Turenne, I. Khmelevskaya, and I. Trubitsyna, Acta Mater. **52**, 4479 (2004).
[27]N. Hatcher, O. Y. Kontsevoi, and A. J. Freeman, Phys. Rev. B **79**, 020202(R) (2009).
[28]N. Hatcher, O. Y. Kontsevoi, and A. J. Freeman, Phys. Rev. B **80**, 144203 (2009).
[29]K. Parlinski and M. Parlinska-Wojtan, Phys. Rev. B **66**, 064307 (2002).
[30]X.-Q. Wang, Phys. Rev. B **78**, 092103 (2008).
[31]Z.-Y. Zeng, C.-E. Hu, L.-C. Cai, X.-R. Chen, and F.-Q. Jing, Physica B **405**, 3665 (2010).
[32]J.-M. Lu, Q.-M. Hu, and R. Yang, Acta Mater. **56**, 4913 (2008).
[33]M. F.-X. Wagner and W. Windl, Acta Mater. **56**, 6232 (2008).
[34]M. F.-X. Wagner and W. Windl, Scripta Mater. **60**, 207 (2009).
[35]D. C. Swift, J. G. Niemczura, D. L. Paisley, R. P. Johnson, A. Hauer, R. E. Hackenberg, J. Cooley, D. Thoma, and G. J. Ackland, J. Appl. Phys. **98**, 093512 (2005).
[36]Z.-Y. Zeng, C.-E. Hu, L.-C. Cai, X.-R. Chen, and F.-Q. Jing, Solid State Commun. **149**, 2164 (2009).
[37]G. Herget, M. Müllner, J. B. Suck, R. Schmidt, and H. Wipf, Europhys. Lett. **10**, 49 (1989).
[38]G. L. Zhao and B. N. Harmon, Phys. Rev. B **48**, 2031 (1993).
[39]S. Taioli, C. Cazorla, M. J. Gillan ,and D. Alfè, Phys. Rev. B **75**, 214103 (2007).
[40]C. Cazorla, M. J. Gillan, S. Taioli, and D. Alfè, J. Chem. Phys. **126**, 194502 (2007).
[41]X. W. Zhou, H. N. G. Wadley, R. A. Johnson, D. J. Larson, N. Tabat, A. Cerezo, A. K. Petford-Long, G. D. W. Smith, P. H. Clifton, R. L. Martens, and T. F. Kelly, Acta Mater. **49**, 4005 (2001).
[42]X. W. Zhou, R. A. Johnson, and H. N. G. Wadley, Phys. Rev. B **69**, 144113 (2004).
[43]R. A. Johnson, Phys. Rev. B **39**, 12554 (1989).
[44]P. Sittner, P. Lukás, D. Neov, V. Novák, and D. Toebbens, J. Phys. IV **112**, 709 (2003).
[45]O. Mercier, K. N. Melton, G. Gremand, and J. Hägi, J. Appl. Phys. **51**, 1833 (1980).
[46]J. Uchil, K. P. Mohanchandra, K. G. Kumara, K. K. Mahesh, and T. P. Murali, Physica B **270**, 289 (1999).
[47]L. Chudinovskikh and R. Boehler, Earth. Planet. Sci. Lett. **257**, 97 (2007).
[48]R. Boehler, Phys. Earth Planet. Inter. **96**, 181 (1996).
[49]See http://www.crct.polymtl.ca/FACT/ for more information on Ni-Ti system Phase Diagram (from SGTE 2007 Alloy database).
[50]T. B. Massalski, H. Okamato, P. R. Subramanian, and L. Kacprzak, *Binary Alloy Phase Diagrams* (ASM International, Ohio, 1990).
[51]D. A. Young, *Phase Diagrams of the Elements* (University of California Press, Berkeley, 1991).
[52]C.-E. Hu, Z.-Y. Zeng, L. Zhang, X.-R. Chen, L.-C. Cai, and D. Alfè, J. Appl. Phys. **107**, 093509 (2010).
[53]F. Luo, X.-R. Chen, L.-C. Cai, and G.-F. Ji, J. Chem. Eng. Data **55**, 5149 (2010).
[54]S.-N. Luo and T. J. Ahrens, Phys. Earth Planet. In. **143**, 369 (2004).
[55]S.-N. Luo and T. J. Ahrens, Appl. Phys. Lett. **82**, 1836 (2003).